UNIFYING THE RANDOM WALKER ALGORITHM AND THE SIR MODEL FOR GRAPH CLUSTERING AND IMAGE SEGMENTATION

Christos G. Bampis [1] *and Petros Maragos* [2]

[1] Department of Electr. and Computer Eng., University of Texas at Austin, Austin, TX 78712-0240, USA.
[2] School of Electr. and Computer Eng., National Technical University of Athens, 15773 Athens, Greece.
bampis@utexas.edu, maragos@cs.ntua.gr

ABSTRACT

In this paper, we explore the image segmentation task using a graph clustering approach. We formulate this clustering as a diffusion scheme whose steady state is determined by the Random Walker (RW) method. Then, we discover the equivalence of this diffusion with the Susceptible - Infected - Recovered (SIR) model, a well-studied epidemic propagation model. We further argue that using a Region Adjacency Graph (RAG) exploits the clustering properties and leads to a dimensionality reduction. Finally, we propose a novel method called Normalized Random Walker (NRW) algorithm which extends the RW method. Qualitative and quantitative experiments validate the efficiency and robustness of our method, with respect to parameter tuning, seed quality and location.

Index Terms— graph clustering, Random Walker, SIR epidemic propagation model, diffusion modeling, image segmentation

1. INTRODUCTION

Image segmentation is broadly studied in image analysis and computer vision and provides useful information for various applications, such as object detection or image retrieval. Lately, there has been an increased interest for graph-based methods where the image is being treated as a graph with nodes placed in every pixel or region. Some well-known methods have proposed energy minimization using an eigenvalue problem solution [22] or a graph cut solution via a max-flow algorithm [4]. In [13], Grady proposed the Random Walker (RW) method, which was further extended and developed thereafter for various applications, as in [8], [31], [20] and [11].

In this work, we propose an improvement of the RW by exploring the underlying diffusion schemes and discovering a novel connection with the SIR model. In Section 2, we make all the definitions used throughout this work. In Section 3, we briefly describe the RW method and in Section 4 we describe the SIR model and prove its connection with the RW method. Then, Section 5 proposes the Normalized Random Walker (NRW) method, whereas Section 6 discusses the need of using an image-driven graph (RAG) instead of a regular grid. Finally, Section 7 presents and discusses our experimental results and Section 8 summarizes the important conclusions.

2. BACKGROUND

Let $G = (V, E)$ denote a graph consisting of a set of vertices (nodes) $v \in V$ and a set of edges $e \in E \subseteq V \times V$. In addition, an edge e_{ij} denotes an edge spanning two vertices v_i and v_j. In order to represent node similarity we use a weighted version of G by defining non-negative weights w_{ij} between nodes i and j. Similarly, the degree of node i is $d_i = \sum_{j \sim i} w_{ij}$, where $\sim$ denotes that i and j are adjacent. In addition, we define the weight matrix $W = [w_{ij}]$ and the degree matrix $D = \mathrm{diag}(d_1, \ldots, d_n)$, where $n = |V|$. We also assume that G is connected and undirected ($w_{ij} = w_{ji}$).

The construction of the weight matrix W is an important step for the final segmentation. In most cases, a Gaussian kernel with parameter σ is used:

$$w_{ij} = \begin{cases} \exp\left[-\left(\frac{\|\mathbf{g}_i - \mathbf{g}_j\|_2}{\sigma}\right)^2\right], & \text{if } j \sim i \\ 0, & \text{else} \end{cases} \quad (1)$$

where $\mathbf{g}_i$ is the feature vector (e.g. a 3-D RGB vector) for node i. Other weighting factors were studied in [12], [16].

3. RANDOM WALKER

In [13], Grady proposed the RW algorithm, where the user inputs a set of seeds, each belonging to a set of N_s possible labels $\{s_i\}$, $i = 1, \ldots, N_s$. This set of marked pixels is then used to extract the desired object boundaries. The final segmentation is interpreted as the most probable label s of each node, i.e. which type of seed is the most probable final destination for a random walker who starts his trip from every unmarked node. According to [13], the direct solution of the random walker's probabilities with respect to all unmarked nodes, is computationally intractable. Instead, one may solve the relevant Dirichlet problem (also known as combinatorial Dirichlet integral for graph applications) [7], [10] and apply the RW algorithm. We now briefly describe the algorithm. Suppose L is the unnormalized graph Laplacian [13]:

$$L = D - W = [l_{ij}] = \begin{cases} d_i, & \text{if } i = j \\ -w_{ij}, & \text{if } j \sim i \\ 0, & \text{else} \end{cases} \quad (2)$$

Then the minimization of $J(\mathbf{x})$, where

$$J(\mathbf{x}) = \frac{1}{2} \sum_{i,j=1}^{N} w_{ij} \Big(x_i - x_j\Big)^2 = \frac{1}{2} \mathbf{x}^\top L \mathbf{x} \quad (3)$$

given the constraints (seed locations) encoded in $\mathbf{x} = [x_i]$, provides the solution. To effectively minimize J, one must solve a set of linear systems. Finally, for every unmarked node, one picks the label that corresponds to the maximum probability. An interesting property that arises when minimizing J is that the resulting probabilities are well-defined, i.e. for every node the sum across all labels is 1. More

Most of this work was done at NTUA. It was partially supported by the project COGNIMUSE which is implemented under the ARISTEIA Action of the Operational Program Education and Lifelong Learning and is co-funded by the European Social Fund and Greek National Resources. It was also partially supported by the European Union under the projects MOBOT with grant FP7-600796 and DIRHA with grant FP7-288121.

importantly, the RW algorithm is directly related to the steady state of the heat diffusion equation [13], [27]: $\frac{du}{dt} = \nabla^2 u$.

There have been many extensions to the RW algorithm. As an example in [14], prior models were introduced to effectively detect object parts that are not connected to a seed. Also, the use of filterbank features have been proposed in [3] for texture segmentation. Finally, the use of an over-segmentation step to effectively decrease the number of nodes was studied in [18], [23] and pre-computation techniques were used in [2] to achieve a computational speedup.

As with most seeded segmentation methods, RW is sensitive to initial seed location, number and quality when the human factor introduces incorrect initial seeds (outliers) due to lack of expertise or concentration. There has been some work on intelligent seed choice with interesting results [26]. Parameter tuning is also an important aspect, since prior knowledge of σ is usually unavailable and can vary from image to image. Searching for an optimal σ iteratively or computing it explicitly [12] usually adds computational time.

4. SIR MODEL

The diffusive nature of the RW can be thought of as the evolution of heat flowing in a graph [27] or as a label propagation effect for graph-based learning applications [25], [30]. Alternatively, one can consider this diffusion as a propagation of infection waves originating from "breakout" points. These infection waves travel through a network of nodes or people according to node similarity: nodes that are strongly connected should influence one another at a higher rate compared to those weakly connected. A real life analog could be that friendships among members of a community share more experiences and are more prone to be infected from someone they spend more time with, use the same objects, etc.

A well-known model for the evolution of such an epidemic spread is the Susceptible - Infected - Recovered (SIR) model [15], [21]. According to [21], it is a model describing the infection spread on stationary people (nodes) belonging in a fixed size community. This community consists of three compartments: those who are susceptible (S) to an infection, those already infected (I) and those who recovered from it after infection (R). Also, the community is represented by a regular grid of 4 neighbors for each person. Let $I(x, y)$ denote the probability of a person in location (x, y) to be infected and $S(x, y)$ the probability of being susceptible. Then, this evolution can be expressed through the following equation:

$$\Delta I(x,y) = \frac{k}{4} S(x,y)(4I(x,y) + a^2 \nabla^2 I(x,y))\Delta t \qquad (4)$$

where ΔI is the increase of $I(x, y)$ per time step Δt, k is the rate of influence for all of this person's neighbors and a is the distance between every person and its neighbor in the community.

We reformulate this model to accommodate our work and prove that the SIR model is equivalent to the following diffusion model[1]:

$$I_{i,t+1} = I_{i,t} + \sum_{j \sim i} \partial_j I_{i,t} \qquad (5)$$

where i, j denote the respective nodes, t is the iteration index and $\partial_j I_{i,t} = w_{ij}(I_{j,t} - I_{i,t})$. We define $I_{i,t}$ to be the corresponding infection probability of node i at time step t, which is increased by $\Delta I_{i,t}$ during each time step. We normalize time steps ($\Delta t = 1$), omit the compartment R and consider all nodes to be equally susceptible to all infections regardless of their location and time, since we only care about infection waves and their superiority over each node. To model node similarity we replace $\frac{k}{4}$ with $\frac{w_{ij}}{d_i}$, i.e. we average node similarity between i and j. In order to reach a well-defined steady state (4) needs to be reformulated. In other words, the steady state corresponds to $\Delta I_i = 0$, i.e. we are no longer updating infection probabilities at any node i centered at location (x, y). By making use of the harmonic property [27], we redefine (4) as

$$\Delta I_{i,t} = \sum_{j \sim i} w_{ij}(I_{j,t} - I_{i,t}) = \sum_{j \sim i} w_{ij} I_{j,t} - I_{i,t} d_i \qquad (6)$$

Then, we get (5) from (6) and the fact that $\Delta I_{i,t} = I_{i,t+1} - I_{i,t}$.

5. NORMALIZED RANDOM WALKER

By carefully analyzing (5), we can observe that the degree of the nodes is not taken into account when computing the edge derivative. However, this would not be natural in a real-life example: the number of neighbors each person has influences the local infection profile. Suppose that A has 2 friends, B and C. Also, suppose that both of them are equally friends to A, but B has more friends than C. Then, B will influence more A' s infection profile. In other words, the probability of a node's infection is related to its degree and that of his neighbors. We propose to incorporate degree terms to satisfy this observation. Denote the normalized graph Laplacian [28], [29] by $\tilde{L} = D^{-\frac{1}{2}}(D - W)D^{-\frac{1}{2}} = [\tilde{l}_{ij}]$, where

$$\tilde{l}_{ij} = \begin{cases} 1, & \text{if } i = j \\ -\frac{w_{ij}}{\sqrt{d_i d_j}}, & \text{if } j \sim i \\ 0, & \text{else} \end{cases} \qquad (7)$$

We also define the normalized derivative over edge e_{ij} as

$$\partial_j I_{i,t} = \frac{w_{ij}}{\sqrt{d_i}} \left(\frac{I_{j,t}}{\sqrt{d_j}} - \frac{I_{i,t}}{\sqrt{d_i}} \right) \qquad (8)$$

Then, by plugging (8) to (5) we can define a new steady state which (by following the same steps as before) minimizes $J_n(\mathbf{x})$, a normalized version of $J(\mathbf{x})$, where

$$J_n(\mathbf{x}) = \frac{1}{2} \sum_{i,j=1}^{N} w_{ij} \left(\frac{x_i}{\sqrt{d_i}} - \frac{x_j}{\sqrt{d_j}} \right)^2 \qquad (9)$$

We can now minimize $J_n(\mathbf{x})$ by solving a similar set of linear systems as in the traditional algorithm. In fact, we omit the constraints that were present in the original idea: we relax the resulting probabilities to non-negative numbers which reveal the certainty of each label without satisfying the maximum principle. As a result, all N_s linear systems (or infections present) have to be solved. In the RW method we only solve $N_s - 1$ systems since the transition probabilities sum to 1.

6. REGION ADJACENCY GRAPH FOR CLUSTERING

Instead of applying our algorithm on a pixel level (regular grid), we propose to extend our method to a Region Adjacency Graph (RAG - [23]). In other words, we can use any over-segmentation technique (such as watershed transformation - [19]) and therefore obtain a set of n regions $R_1, R_2, ..., R_n$ which are now represented by a node i, located at the geometric mean $\mathbf{h}_i$ of R_i and whose feature vector is $\mathbf{g}_i$, i.e. the mean feature vector for all pixels in R_i. Consequently, we can greatly reduce the problem's dimensionality. We also prefer the node-level approach, since it better approximates real-life situations, where the number of friends or neighbors for each person is free of spatial regularity. We also note that in this case the degree of each node will be more accurately depicting the

[1] The steady state for this evolution is identical to the RW solution, since the SIR model belongs to the class of local mean field models [21].

relationship between adjacent regions, thus capturing the internal structure more accurately. A drawback of the RAG is that we need to interpret the initial seeds in terms of their corresponding nodes. A good approximation is to assign each seed's label to the node closest to the seed's pixel, by assuming that the user will not input any seeds very close to an object's boundary. A more accurate (but slower) approach would be to assign the seed's label to the region or node this pixel belongs to. Furthermore, to turn the node solution into a pixel one, we have to assign all pixels in R_i to label s_i. Finally, we deal with boundary pixels by assigning each one to the most common label present with respect to this pixel's eight neighbors. In the quantitative results we use the node level solution for efficiency.

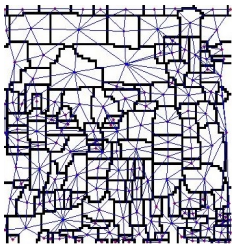

Fig. 1: Region Adjacency Graph (RAG)

7. EXPERIMENTAL RESULTS

In our experiments, we use the RAG version of the RW/NRW since its arbitrary graph structure is heavily exploited by the degree term of the NRW and demonstrates our graph clustering approach. Our data consists of 24 images from the Berkeley dataset and 30 images from the Grabcut Microsoft Research dataset. All images were chosen so that a main object was present and a 2-seeds/infections model would be applicable. We also used some other images from the Berkeley dataset for a 3/4-seeds model for qualitative results.

Table 1: Graph-based segmentation F-scores: Berkeley Dataset

		RW	NRW	LC	GC
RGB	mean	0.7460	0.7767	0.7288	0.6673
	std	0.1472	0.1399	0.1652	0.2614
Gray	mean	0.7264	0.7563	0.7215	
	std	0.1585	0.1489	0.1671	
Luv	mean	0.7383	**0.7791**	0.7415	
	std	0.1455	**0.1319**	0.1584	

Table 2: Graph-based segmentation F-scores: Grabcut Dataset

		RW	NRW	LC	GC
RGB	mean	0.5960	0.6554	0.5615	0.5531
	std	0.1606	0.1548	0.1662	0.2490
Gray	mean	0.5875	0.6404	0.5593	
	std	0.1795	0.1688	0.1746	
Luv	mean	0.5897	**0.6664**	0.5891	
	std	0.1545	**0.1493**	0.1674	

According to Tables 1 and 2, the NRW produces better segmentation results on average in both datasets. Using Luv features also improved the final NRW average. The relative differences are more important than the absolute values, since we are taking an average over non-optimal values of σ, 10 different manual segmentations and across all images of the respective image set. The standard deviation for the NRW is smaller than the RW one which suggests that the NRW is more robust. Initial seed points were manually placed for all images in moderation. The σ parameter was chosen in the $[30, 150]$ interval, since for each image the optimal value varies. We also used only color information to construct the weight matrix. Finally, to produce the F-scores, we used ground truth masks of the images and turned them into the respective node level solution. Then, we calculated an approximated version of the F-scores using the reference solution and the RW/NRW ones. In practice, this approximation was close enough to its pixel version and much faster. For comparison reasons, we applied the methods from [9] (LC) and [17] (GC) using the available codes. The LC pixel-level method usually produces slightly lower results than the node-level RW. We experimented with all graph-cut methods from [17] using default parameters and k-means, where much better results were obtained for many cases. However, leakage effects and seed number sensitivity led to large inter-image and intra-image variability. Results using RGB only were available and we took an average over all methods used in [17], since for these seeds we got similar results. Finally, we used the GrowCut technique [24], but it produced poor results for the same seed choices. Quantitative results are presented in Figs. 2, 3, 4.

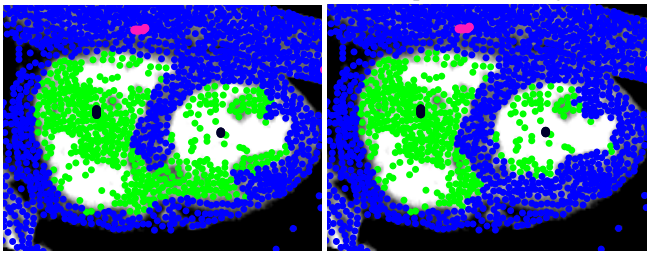

Fig. 2: 2-seeds model, $\sigma = 90$, RW (left), NRW (right), graph clustering

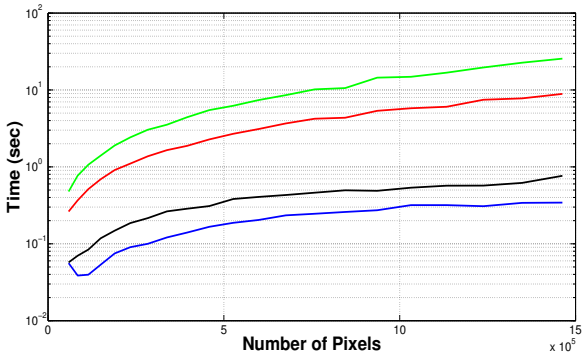

Fig. 3: green: NRW no RAG, red: RW no RAG, black: NRW with RAG and blue: RW with RAG

Figure 2 shows the node solution on a CT image after applying the two methods. We define two types of seeds/infections (black and pink dots), map them to nodes and perform clustering on the resulting RAG using the RW and the NRW. Figure 3 shows that the NRW adds a relatively small computational burden (compute $D^{-\frac{1}{2}}$ and perform multiplications) especially after using the RAG dimensionality reduction. The advantage of the RAG is twofold: not only it models more complex relations between pixels, but it also greatly reduces the problem's dimension. We note that using the RAG in conjunction with our SIR analysis supports the theoretical merits of using a normalized graph Laplacian [6].

8. CONCLUSIONS

In this work, we proposed a novel modification to the RW algorithm. To do so, we considered the solution of the RW as the steady state of infectious diseases propagating on an image-driven graph. By carefully analyzing the SIR epidemic model, we discovered an equivalence between these two approaches, which revealed the need to incorporate degree terms to normalize over each infection's probability. In practice, the NRW achieved better segmentation results in many challenging occasions. Our ongoing and future work includes investigating other superpixel methods to create RAGs (e.g. [1]), using prior models [14] or using alternative features like texture.

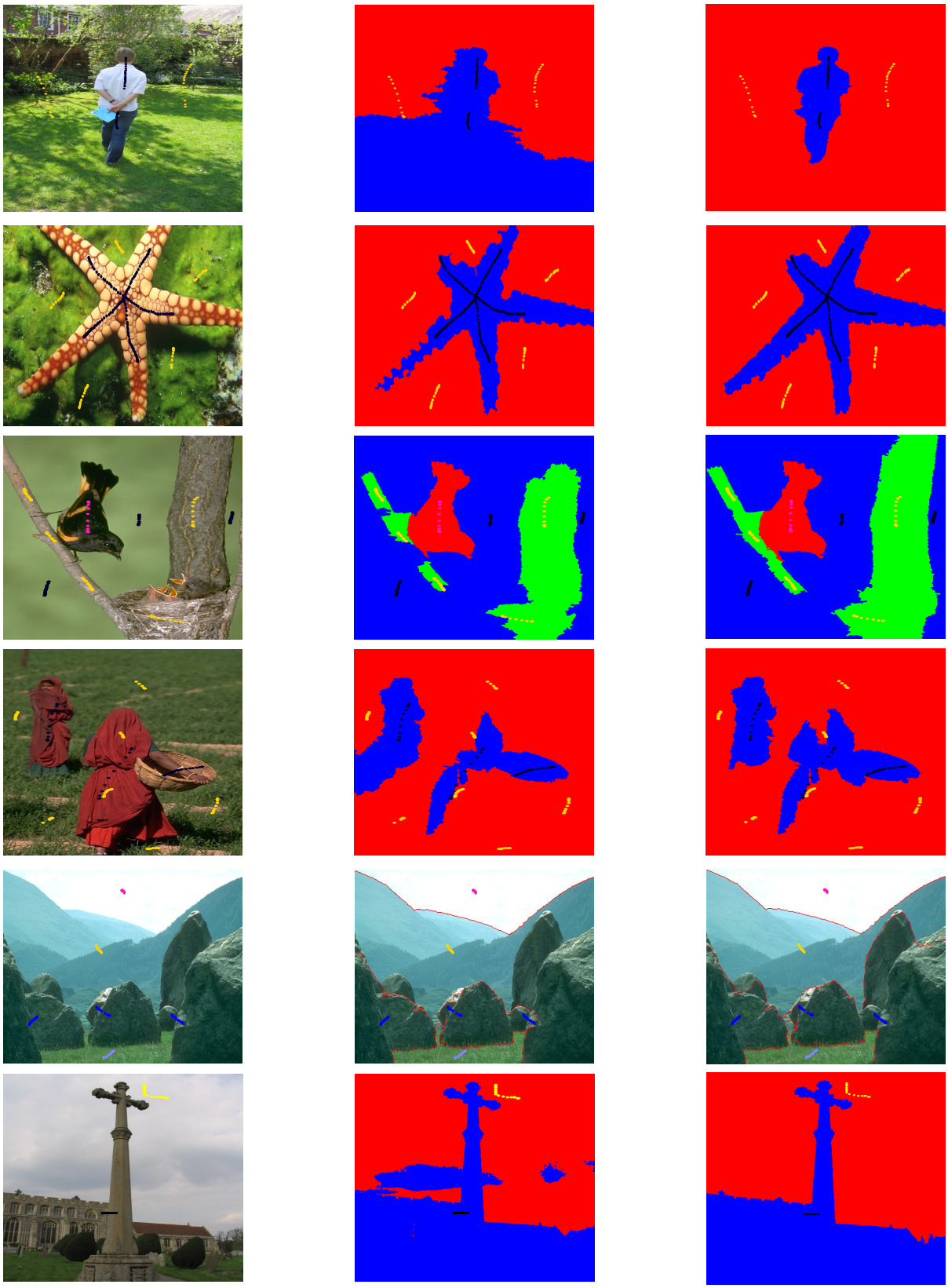

Fig. 4: Pixel level results (labels/boundaries) using the node solution. Column 1 is the original images with seeds as colored dots. Column 2 (rows 1-5) is the RW, column 2 (row 6) is GC (the first one from [17]) where leakage effect is present and column 3 is the NRW. Rows 1, 2 and 3 present results for 2 and 3 types of seeds/infections. In row 4, outliers are introduced and the NRW locates both women better. Row 5 shows the boundaries in a 4-seeds model with a much better result for the NRW. RW/NRW experiments use $\sigma = 90$ (except for column 3 - row 6 where $\sigma = 30$ is used). This figure is better seen in color.

9. REFERENCES

[1] R. Achanta et al., "SLIC superpixels compared to state-of-the-art superpixel methods", IEEE Transactions on Pattern Analysis and Machine Intelligence, vol. 34, no. 11, pp. 2274-2282, Nov. 2012.

[2] S. Andrews, G. Hamarneh and A. Saad, "Fast random walker with priors using precomputation for interactive medical image segmentation", Proc. of Medical Image Computing and Computer Assisted Intervention (MICCAI), pp. 9-16, 2010.

[3] Y. Artan and I. Yetik, "Improved Random Walker Algorithm for Image Segmentation", Proc. of the IEEE Southwest Symposium on Image Analysis and Interpretation (SSIAI), pp. 89-92, May 2010.

[4] Y. Boykov and M. P. Jolly, "Interactive graph cuts for optimal boundary and region segmentation of objects in N-D images", Proc. of the International Conference on Computer Vision (ICCV), pp. 105-112, 2001.

[5] Y. Boykov and V. Kolmogorov, "An Experimental Comparison of Min-Cut/Max-Flow Algorithms for Energy Minimization in Vision", IEEE Transactions on Pattern Analysis and Machine Intelligence, vol. 26, no. 9, pp. 1124-1137, Sep. 2004.

[6] F. R. K. Chung, "Spectral Graph Theory", Providence, RI, USA: American Mathematical Society, 1997.

[7] R. Courant and D. Hilbert, *Methods of Mathematical Physics*, John Wiley and Sons, vol. 2, 1989.

[8] C. Couprie, L. Grady, L. Najman and H. Talbot, "Power Watershed: A Unifying Graph-Based Optimization Framework", IEEE Transactions on Pattern Analysis and Machine Intelligence, vol. 33, no. 7, pp. 1384-1399, Jul. 2011.

[9] W. Casaca, L. G. Nonato and G. Taubini, "Laplacian Coordinates for Seeded Image Segmentation", Proc. IEEE Conference Computer Vision Pattern Recognition (CVPR), pp. 384-391, Jun. 2014.

[10] P. Doyle and L. Snell, "Random walks and electric networks", ser. *Carus mathematical monographs*, Mathematical Association of America, no. 22, 1984.

[11] M. D. Collins, X. Jia, L. Grady and V. Singh, "Random walks based multi-image segmentation: Quasiconvexity results and GPU-based solutions", Proc. IEEE Conference Computer Vision Pattern Recognition (CVPR), pp. 1656-1663, Jun. 2012.

[12] A. Elmoataz, O. Lezoray and S. Bougleux, "Nonlocal discrete regularization on weighted graphs: A framework for image and manifold processing", IEEE Transactions on Image Processing, vol. 17, no. 7, pp. 1047-1060, Jul. 2008.

[13] L. Grady, "Random walks for image segmentation", IEEE Transactions on Pattern Analysis and Machine Intelligence, vol. 28, no. 11, pp. 1768-1783, Nov. 2006.

[14] L. Grady, "Multilabel random walker image segmentation using prior models", Proc. of the IEEE Computer Society Conference on Computer Vision and Pattern Recognition (CVPR), vol. 1, pp. 763-770, Jun. 2005.

[15] H. W. Hethcote, "The mathematics of infectious diseases", SIAM Review, vol. 42, no. 4, pp. 599-653, 2000.

[16] Y. L. Khai and R. Mandava, "Random walker with improved weighting function for interactive medical image segmentation", Bio-Medical Materials and Engineering Journal, vol. 24, no. 6, pp. 3333-3341, 2014.

[17] P. Kohli, A. Osokin and S. Jegelka, "A Principled Deep Random Field Model for Image Segmentation", Proc. of the IEEE Computer Society Conference on Computer Vision and Pattern Recognition (CVPR), pp. 1971-1978, Jun. 2013.

[18] G. Li, L. Qingsheng and C. Jian, "A New Fast Random Walk Segmentation Algorithm", Proc. of the 2nd International Symposium on Intelligent Information Technology Application, Shanghai, pp. 693-697, 2008.

[19] F. Meyer, "Topographic distance and watershed lines", Signal Processing, vol. 38, no.1, pp. 113-125, Jul. 1994.

[20] T. Patz and T. Preusser, "Segmentation of Stochastic Images With a Stochastic Random Walker Method", IEEE Transactions on Image Processing, vol. 21, no. 5, pp. 2424-2433, May 2012.

[21] E. Postnikov and I. Sokolov, "Continuum description of a contact infection spread in a SIR model", Mathematical Biosciences 208, pp. 205-215, 2007.

[22] J. Shi and J. Malik, "Normalized cuts and image segmentation", IEEE Transactions on Pattern Analysis and Machine Intelligence, vol. 22, no. 8, pp. 888-905, Aug. 2000.

[23] A. Tremeau and P. Colantoni, "Region adjacent graph applied to color image segmentation", IEEE Transactions on Image Processing, vol. 9, pp. 735-744, 2000.

[24] V. Vezhnevets and V. Konouchine, "GrowCut - interactive multi-label N-D image segmentation by cellular automata", Proc. 15th Int. Conf. on Comp. Graphics and Appl. GraphiCon, Novosibirsk, Russia, pp. 150-156, 2005.

[25] F. Wang and C. Zhang, "Label Propagation through Linear Neighborhoods", IEEE Transactions on Knowledge and Data Engineering, vol. 20, no. 1, pp. 55-67, Jan. 2008.

[26] W. Yang, J. Cai, J. Zheng and J. Luo, "User-Friendly Interactive Image Segmentation Through Unified Combinatorial User Inputs", IEEE Transactions on Image Processing, vol. 19, no. 9, pp. 2470-2479, Sep. 2010.

[27] X. Zhu, Z. Ghahramani and J. Lafferty, "Semi-supervised learning using Gaussian fields and harmonic functions", Proc. of the 20-th International Conference on Machine Learning (ICML), 2003.

[28] D. Zhou, O. Bousquet, T. Lal, J. Weston and B. Scholkopf, "Learning with Local and Global Consistency", Proc. of NIPS, 2003.

[29] D. Zhou and B. Scholkopf, "Learning from Labeled and Unlabeled Data Using Random Walks", Proc. of the 26th DAGM Symposium, 2004.

[30] X. Zhu and Z. Ghahramani, "Learning from labeled and unlabeled data with label propagation", Technical Report 02-107, CMU-CALD, Carnegie Mellon University, Jun. 2002.

[31] J. Zhang, J. Zheng and J. Cai, "A diffusion approach to seeded image segmentation", Proc. IEEE Conference Computer Vision Pattern Recognition (CVPR), pp. 2125-2132, Aug. 2010.